Hindawi
Geofluids
Volume 2020, Article ID 8876400, 11 pages
https://doi.org/10.1155/2020/8876400

Research Article

Permeability Reduction and Electrochemical Impedance of Fractured Rock Grouted by Microbial-Induced Calcite Precipitation

Shuquan Peng,[1] **Kejia Zhang**,[1] **Ling Fan**,[1] **Jingyu Kang**,[2,3] **Kang Peng**,[1] **and Fan Wang**[1]

[1]*School of Resource and Safety Engineering, Central South University, Changsha, Hunan 410083, China*
[2]*State Key Laboratory of Geomechanics and Geotechnical Engineering, Institute of Rock and Soil Mechanics, Chinese Academy of Sciences, Wuhan 430071, China*
[3]*School of Engineering Science, University of Chinese Academy of Sciences, Beijing 100049, China*

Correspondence should be addressed to Ling Fan; pqrfanlinger@csu.edu.cn

Received 28 September 2020; Revised 21 November 2020; Accepted 25 November 2020; Published 8 December 2020

Academic Editor: Zhiming Chen

The poor impermeability of fractured rock induced by excavation and construction is improved through the application of microbial-induced calcite precipitation (MICP), but it is difficult to monitor and evaluate the permeability reduction under a confining pressure and fracture aperture. For this, the grouting ratio, permeability, and electrochemical impedance of fractured rock with MICP grouting were experimented with, considering the effects of fracture aperture and confining pressure. The equivalent circuit model of grouting-fractured rock is presented, and the corresponding ratio of the electrical resistivity and cross-sectional area of the grouted fracture (ρ/S) is indicated by an electrochemical impedance spectroscope (EIS). The relationships of the permeability coefficient, the ρ/S, and the grouting ratio are analysed. The experimental results show that the Darcy permeability coefficient of fractured rock with MICP grouting is reduced by an order of magnitude of 3 to 4. As fracture aperture ranged from 1.28 to 2.56 mm and grouting rate was 0.003 ml/s, the Darcy permeability coefficient decreased with an increase in confining pressure. The grouting ratio and fracture aperture also decreased with a reduction in ρ/S. The results also showed that the permeability reduction of MICP correspondingly increased in these conditions. What is more, the Darcy permeability coefficient of fractured rock grouted by MICP and its permeability reduction may be well predicted by confining pressure and ρ/S. This study provides a new EIS method for predicting the reduction in permeability of MICP grouting-fractured rock and further enriches the application of MICP and EIS techniques in impermeable rock engineering.

1. Introduction

The poor impermeability performance of fractured rock induced by excavation and construction seriously influences the safety of underground engineering projects such as subways and tunnels [1]. Poor impermeability performance is effectively improved by traditional cement-based grouting [2, 3] and polymer grouting [4, 5]. Microbial-induced calcite precipitation (MICP) was elucidated by Mitchell and Santamaria in the 1990s [6] and is a new microbial grouting technique. The MICP technique was applied to the cementation of sands, to enhance bearing capacity and liquefaction resistance, the sequestration of carbon, soil erosion control, groundwater flow control, and the remediation of soil and groundwater impacted by metals [7]. The mechanics of MICP is expressed as follows:

$$CO(NH_2)_2 + 2H_2O + Ca^{2+} \rightarrow {}^{\text{urease}}2NH_4^+ + CaCO_3. \quad (1)$$

Formula (1) shows that the urease secreted by urease-producing bacteria decomposes dissolved urea into carbonate ions, and then cemented calcium carbonate precipitates from the solution, along with carbonate ions and calcium

(a) (b) (c)

Figure 1: Display of experiment samples. (a) Schematic diagram of sample fracture. (b) Picture of samples. (c) The plexiglass strip.

ions. The permeability coefficients of in situ fractured rock and fabricated rock, grouted by MICP, were reduced by 35% and three orders of magnitude, respectively [8–14]. Compared with traditional methods, MICP has low viscosity and grouting pressure, and enables fluid transportation over a longer distance with intrusion into smaller cracks [15, 16]. MICP also has some advantages for environmental protection, such as a moderate pH, small shrinkage, and no release of heavy ions or toxic ions [17, 18].

The reduction in permeability and electrical impedance of MICP grouting-fractured rock can be theoretically determined by its pore structure, and they are affected by factors such as injection rate, bacterial concentration, confining pressure, fracture roughness, and fracture aperture [19–23]. The lower the injection rate, the easier the calcium carbonate precipitation adheres to the fracture surface and the lower the permeability coefficient [24]. The electrical impedance of rock comprises its resistance, capacity, and reactance, and the corresponding electrical impedance spectrum (EIS) technique is a nondestructive method for measuring a rock's water content, porosity, and permeability coefficient [25–30]. However, the reduction in permeability and electric impedance of fractured rock grouted by MICP is affected by confining pressure and fracture aperture, and this is not widely reported.

Therefore, in this paper, the permeability coefficients of prefabricated fractured rocks (before and after MICP grouting) are investigated, as well as their EIS responses. The reduction in permeability caused by confining pressures and fracture apertures is analysed, and the relationships between permeability coefficient, permeability reduction, grouting ratio, and EIS are discussed. The results of this research can further improve MICP application in permeability reduction in underground rock engineering.

2. Experimental Procedures

2.1. Samples and MICP Grouting Solutions. Three cylindrical samples of red sandstone (50 mm diameter and 100 mm height) were selected. Then, three thoroughly fractured rock samples were prefabricated using the Brazilian splitting test, and each fracture aperture was fixed by gluing the split sample to a plexiglass strip, with sizes ranging from 1.0 mm to 2.5 mm (see Figure 1). The physical parameters of the samples (e.g., length (L) and diameter (D_0)) are listed in Table 1.

Table 1: Physical parameters of each sample (unit: 10^{-3} m).

Number	AB	BC	CD	DA	L	D_0	b_a
1-40	48.88	101.14	49.03	101.02	101.08	48.96	1.28
1-32	48.70	100.72	49.12	100.17	100.45	48.91	2.12
1-48	49.12	100.63	49.01	100.24	100.44	49.07	2.56

Note. L is the height of the sample: $L(\mathrm{AD}+\mathrm{BC})/2$; w is the crack length perpendicular to seepage direction: $w(\mathrm{AD}+\mathrm{CD})/2$; b_a is the fracture aperture.

Bacillus *Sporocarsina pasteurii* and cementing solution, mixed with 1 mol/l calcium chloride and 1 mol/l urea, were chosen as MICP grouting solutions. The bacillus *Sporocarsina pasteurii* species was inoculated by 5% in a pH 7.3 fluid nutrient medium, containing urea (20 g/l), soy protein (5 g/l), casein (15 g/l), and sodium chloride (5 g/l). The inoculated bacterial suspension was then cultured in a rotatory shaker at 30°C and 170 rpm for approximately 24 h, until its OD600 and conductivity were 2.4 and 19.5, respectively.

2.2. Experimental Setup. The experimental setup was composed of a self-made seepage device, a MICP grouting device, a rock EIS measuring device, and a triaxial fluid-solid coupled loading system; see Figure 2.

The self-made seepage device was used to test the Darcy permeability coefficients of fractured rock samples without MICP at a constant water head of 17.5 cm [31]. This device was a cylindrical vessel with a diameter of 200 mm and a height of 500 mm that flowed through a 50 mm diameter water outlet connected to the rock sample above the water collector and electronic balance.

The MICP grouting device was used to cement and fill the fractured rock samples. The device had a plexiglass grouting pedestal below the rock sample followed by a plexiglass grouting upper cover with a 3 mm diameter grouting hole linking the bacterial suspension and cementing solution by two rubber grouting pipes of the peristaltic pump WT3000-1JA. The grouting pedestal also had a 3 mm hole to discharge any redundant solution to a waste solution tank.

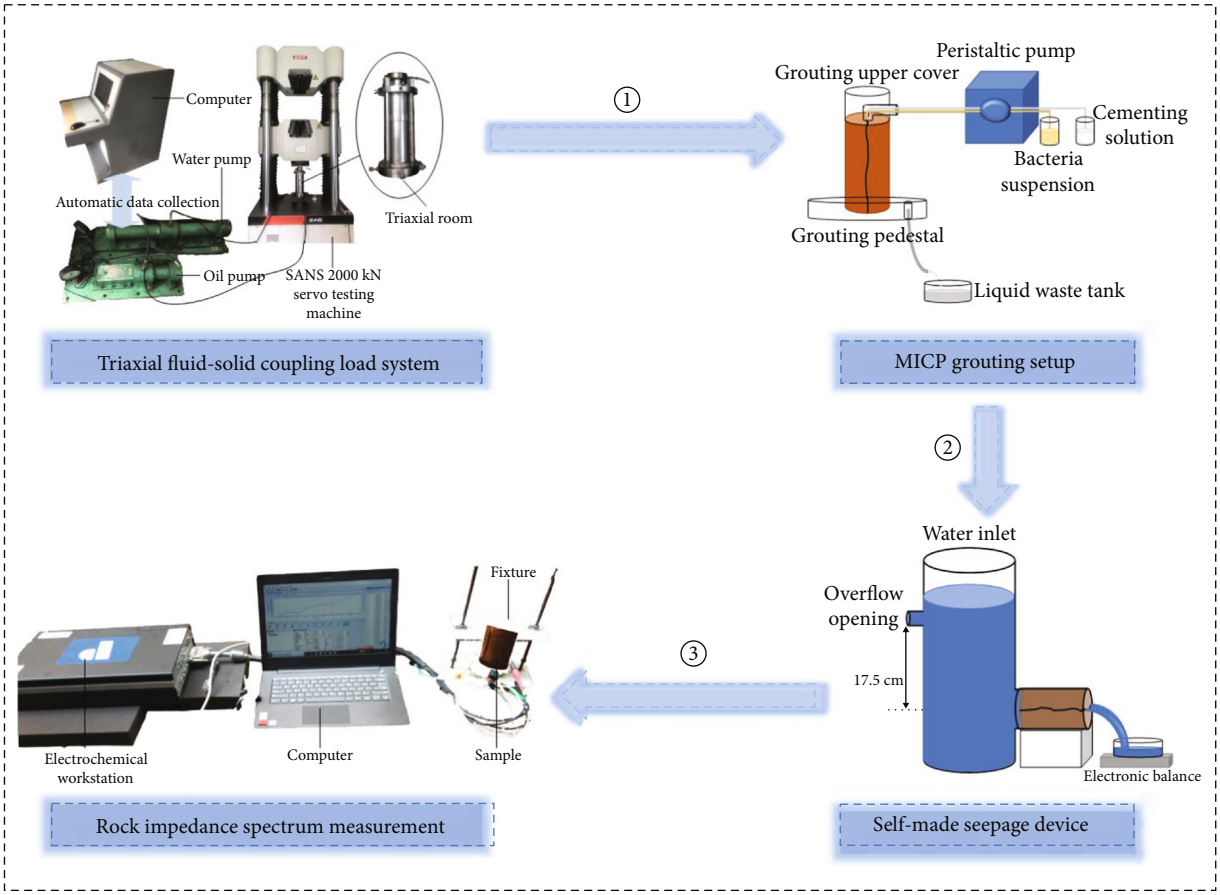

Figure 2: Experimental setup flow chart.

The EIS measuring device was used to measure the electronic impedances of the samples with MICP. The device is comprised of two fixed 8 mm steel columns on a basal steel plate underneath the rock sample, with a dielectric plexiglass upper cover and a movable steel plate pedestal. At the ends of the rock sample, two conductive copper films (with a radius of 30 mm and a thickness of 0.5 mm) were set to connect to the electrochemical workstation (PARSTAT 3000A-DX) by four electrodes.

The triaxial fluid-solid coupled loading system was used to test the Darcy permeability coefficients of fractured rock samples with MICP at constant triaxial loads. This system is a triaxial pressure chamber, applying axial pressure via a SANS 2000 kN servo testing machine. Confining pressure is applied by a servo oil cylinder with a range from 0.01 MPa to 60 MPa; water pressure is applied by a servo water cylinder with a range from 0.01 MPa to 18 MPa.

2.3. Testing Processes. Table 2 lists the cases in this experiment. Firstly, before MICP grouting, the prefabricated, fractured rock samples were weighed and saturated in water for 48 h. Each saturated sample was then horizontally connected to the water outlet of the self-made seepage device at the same height by a wrapped, 55 mm diameter, heat-shrinkable tube, to prevent seepage flowing from the fracture in a longitudinal direction. Continuously adding water into the cylinder vessel kept the water head at 17.5 cm and the seepage was recorded in real time. The Darcy permeability coefficient of each sample was measured without MICP.

Then, each sample was carefully placed between the upper cover and the pedestal of the MICP grouting device, to cause a fracture just below the grouting hole on the upper cover. The peristaltic pump pumped the bacterial suspension

Table 2: Load processes for measuring the permeability coefficient of fractured rock with MICP.

Number	Axial pressure (MPa)	Confining pressure (MPa)	Water pressure (MPa)
1-40	5.0	0.2,0.3,0.4	0.02
1-32	5.0	0.2,0.3,0.4	0.06
1-48	5.0	0.2,0.3,0.4	0.16

Table 3: Microbial quantity of dry samples with and without MICP grouting.

Number	The quantity of sample (g)		m (g)	γ (%)
	Without MICP grouting	With MICP grouting		
1-40	455.82	460.28	4.46	28.16
1-32	465.60	475.03	9.42	36.22
1-48	458.27	480.85	22.58	71.58

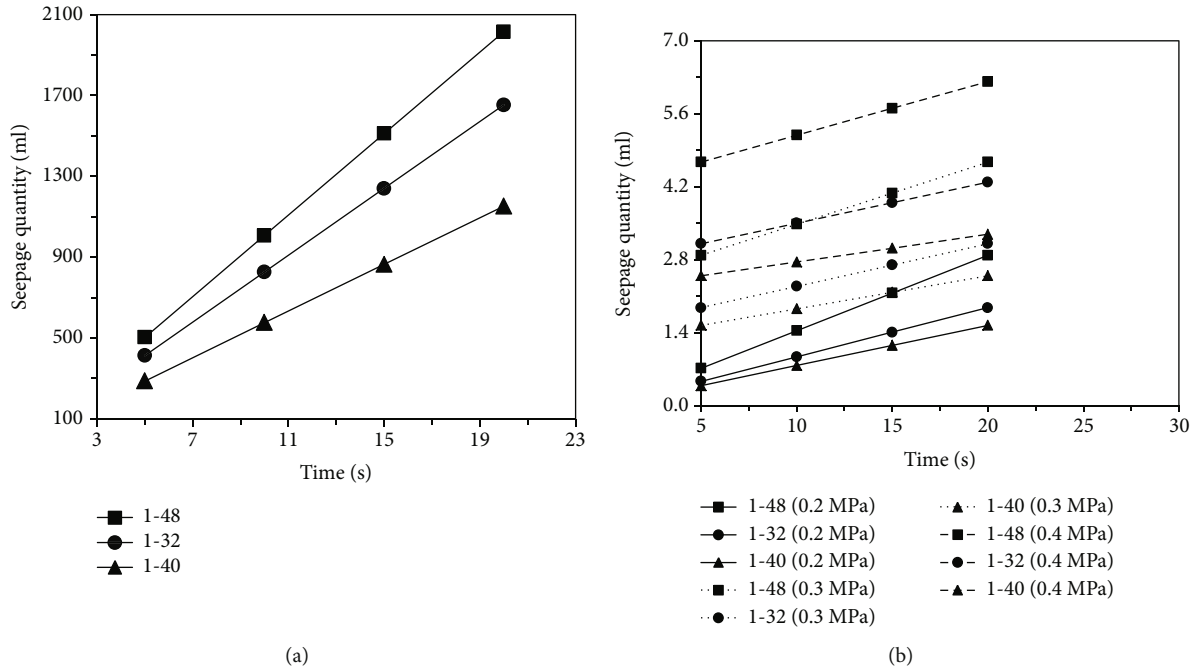

Figure 3: Seepage volume-time relation lines of samples: (a) without MICP and (b) with MICP.

and cementing solution into the fracture until the fracture was full of calcite precipitation, at a given injection rate. The injection rate is important because too slow a rate would greatly increase injection time while too fast a rate would wash away calcium carbonate precipitation in the fracture. Therefore, an injection rate of 0.003 ml/s (corresponding to 3.0 rpm of peristaltic pump speed) was selected. After MICP grouting, each sample was placed in a 70°C drying box for 48 h to stabilise the calcite precipitation, and then weighed again; the grouting ratio of the fractured rock with MICP was calculated.

Next, the Darcy permeability coefficient of each sample with MICP was measured by the triaxial fluid-solid coupled loading system. Before loading, the sample was, again, soaked for 48 h. The sample with the steel upper cover and pedestal on its two ends was wrapped with a 55 mm diameter heat-shrinkable tube to protect the rock sample from oil in the triaxial pressure chamber. The wrapped rock sample was put into the triaxial pressure chamber, and the air in the triaxial chamber and pressure pipes of the loading system was eliminated to reduce testing pressure fluctuation. After this, an axial pressure of 5.0 MPa, a confining pressure of 0.2 MPa, and a water pressure of 0.02 MPa were applied to the sample, in turn, at the given loading rate. The seepage quantity and time were recorded with a frequency of 10 Hz, at the same time. The loading process was repeated for other confining pressures and water pressures (see Table 2).

Afterwards, the electronic impedance of each dry, fractured rock sample with MICP grouting was measured under a 10 mV voltage alternating current (AC) at a frequency range of 10^{-1}-10^{5} Hz. The sample was fixed and connected to the top and bottom copper films, being clamped by the reference electrode and the counter electrode, and by the working electrode and the sense electrode, respectively. After setting the start-up program, the real part and imaginary part of the sample impedance were measured and plotted as a Nyquist diagram fitted with ZView software.

Finally, the relationships among the permeability coefficient, permeability reduction, grouting ratio, and electronic impedance of the fractured rock sample with MICP grouting were analysed.

3. Test Results

3.1. Grouting Ratio of Fractured Rock with MICP. The grouting ratio γ is the ratio of grouting volume to fracture volume of a sample and is calculated by

$$\gamma = \frac{m}{\rho_g L w b_a}, \tag{2}$$

where b_a is the fracture aperture (10^{-3} m), m is the grouted filling quantity (g), and ρ_g is the density of the grouted filling, $\rho_g = 2.5$ g/cm^3. The calculated grouting ratios of each sample with MICP are listed in Table 3.

3.2. Permeability Coefficient and Permeability Reduction of Fractured Rock. Seepage quantity vs. time is plotted in Figure 3. It shows that the seepage quantities of fractured rocks with and without MICP linearly increase with increasing time. So, the seepage flow rates were constant under the constant water pressures and confining pressures listed in Table 2. Therefore, it can be deduced that the seepage of fractured rock samples in this experiment conform to Darcy's law. Darcy's law and the cubic law of seepage can be

presented as follows:

$$Q = \frac{1}{6 \times 10^4} \frac{dV}{dt},$$
$$\frac{Q}{D_0 b} = K \frac{\Delta P}{\rho g L}, \quad (3)$$
$$K = \frac{g b^2}{12u},$$

where Q is the seepage flow rate (m^3/s), and V and t are the seepage quantity (10^{-3} m^3) and time (s), respectively. K is the Darcy permeability coefficient (m/s) of fractured rock samples with MICP and is denoted as K_0 for the sample without MICP grouting, b is the hydraulic aperture of fracture (m), ΔP is water pressure (see Table 2), and u and g are the kinematic viscosity coefficient of water and gravity acceleration, respectively (with magnitudes of 1.0×10^{-6} m^2/s and $10\,m/s^2$).

Substituting equation (3), the hydraulic aperture and the Darcy permeability coefficient of fractured rock without MICP and with MICP become

$$b = 0.2289 \sqrt[3]{\frac{QL}{D_0 \Delta P}},$$
$$K = 438.59 \sqrt[3]{\left(\frac{QL}{D_0 \Delta P}\right)^2}. \quad (4)$$

The calculated K and K_0 are listed in Table 4, and the permeability reduction (K/K_0) is defined as the ratio of K and K_0.

3.3. Impedance of Fractured Rock with MICP. Figure 4 presents the Nyquist graph for the fractured rock sample grouted by MICP. The imaginary part (Zim) is plotted against the real part (Zre) of the fractured rock impedance (Z).

This shows that a tiny arc usually appears in the Nyquist graph at high frequency AC and is followed by a linear segment in the Nyquist graph at low frequency AC. Considering the sample with MICP grouting and its grouting material, the equivalent circuit model of fractured rock with MICP is presented in Figure 5.

The corresponding impedance (Z) is written as follows:

$$Z(\omega) = \mathrm{Zre}(\omega) - j\mathrm{Zim}(\omega) = \mathrm{Rs} + \frac{\mathrm{Rp}}{1 + j\omega \mathrm{CRp}},$$
$$\frac{1}{\mathrm{Rp}} = \frac{1}{\mathrm{Rp}_0} + \frac{1}{\mathrm{Rp}_1} + \frac{1}{\mathrm{Rp}_2}, \quad (5)$$

where j is an imaginary unit, $j^2 = -1$; ω is angular frequency; Rs represents the electrolyte resistance; C represents the electrical double-layer capacitor; and Rp represents the tested resistance. Rp_1 and Rp_2 represent the resistances of two half-fractured rocks and Rp_0 represents the resistance of the sample fracture grouted by MICP.

Table 4: The Darcy permeability coefficients of samples without and with MICP.

Number	K_0 without MICP (10^{-3} m/s)	K with MICP (10^{-3} m/s)		
	0.0 MPa	0.2 MPa	0.3 MPa	0.4 MPa
1-40	727.35	2.26	1.98	1.76
1-32	922.47	1.03	0.94	0.91
1-48	1051.61	0.67	0.60	0.54

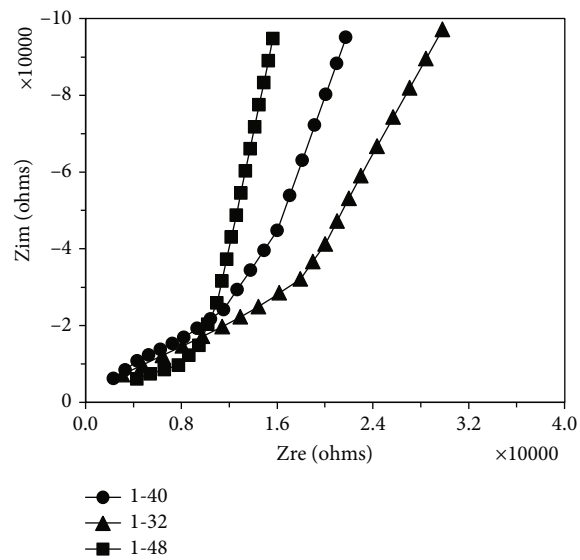

Figure 4: Nyquist graph of samples with MICP.

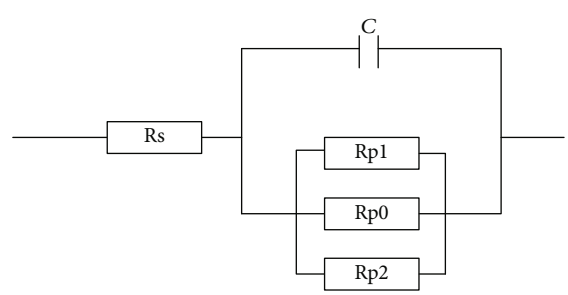

Figure 5: Equivalent circuit model diagram.

Based on Figure 5 and equation (5), the Rp, Rs, and C of the fractured rock sample with MICP were well fitted by ZView 2.0 software and are shown in Table 5. In Table 5, ρ/S is the ratio of electrical resistivity of the MICP-filled fracture (ρ) and the area of the cross-section of the fracture (S); it is calculated by:

$$\frac{\rho}{S} = \frac{\mathrm{Rp}_0}{L}, \quad (6)$$

4. Analyses and Discussion

4.1. Effect of Confining Pressure on Seepage Permeability Coefficient and Permeability Reduction. Figure 6 shows the Darcy permeability coefficient of fractured rock without

Table 5: Parameters after curve fitting of an equivalent circuit model.

Number	Rs	C	Rp_1	Rp_0	Rp_2	ρ	ρ/S
1-40	1964	$3.25E-11$	239960	131111.5	258910	81288.09	1297.11
1-32	1855	$3.21E-11$	176850	85313.22	213540	88064.31	849.31
1-48	2684	$4.66E-11$	141510	46498.77	149820	58155.49	462.95

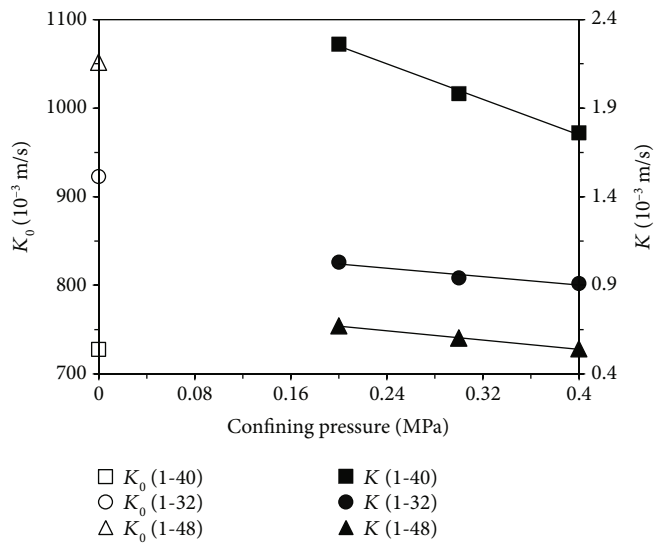

Figure 6: Effect of confining pressure on the permeability coefficient of fractured rock.

MICP (K_0) and with MICP (K) versus confining pressure. When the confining pressure increased from 0.2 MPa to 0.4 MPa (at increments of 0.1 MPa), the Darcy permeability coefficient of three samples linearly declined. This indicates that confining pressure obviously reduces the permeability coefficient of MICP for fractured rock.

Figure 7 plots the permeability reduction (K/K_0) versus confining pressure. The Darcy permeability coefficient decreased by three to four orders of magnitude due to MICP. The permeability reduction also decreased, with increasing confining pressure. It was concluded that the increase of confining pressure increased permeability reduction of MICP. Therefore, the existence of confining pressure, ranging from 0.2 MPa to 0.4 MPa, benefited the MICP technique in achieving a better permeability reduction for fractured rock. Ma et al. [20] analysed the seepage properties of fractured rocks under different confining pressures. When confining pressure was below 10-12 MPa, the permeability coefficient decreased exponentially, as confining pressure gradually increased and then decreased in a slow drop under higher confining pressure. Moreover, the analysis of experimental data in this paper was consistent with [20]; it was concluded that increasing confining pressure within the test range (low confining pressure environment) effectively enhanced the impermeability performance effect of fractured rock with MICP.

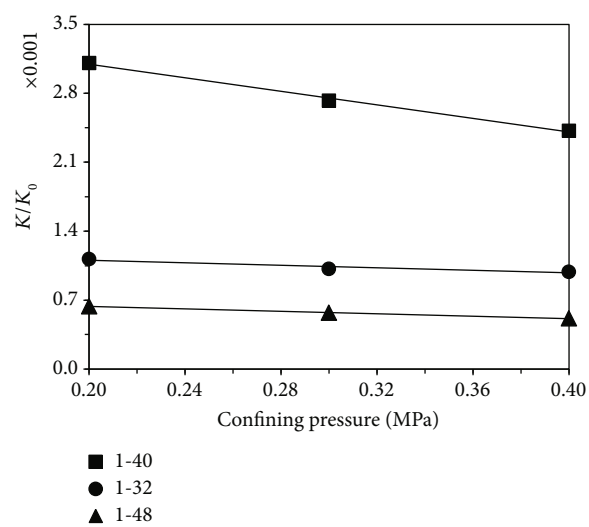

Figure 7: Effect of confining pressure on permeability reduction of fractured rock.

4.2. Effect of Fracture Aperture on Grouting Ratio, Permeability Coefficient, and Permeability Reduction. The MICP grouting ratio (γ) of the samples vs. the fracture aperture (b_a) is shown in Figure 8. When the fracture apertures of three samples ranged from 1.28 mm to 2.56 mm, the grouting ratios increased with an increase in fracture aperture. This is because the increase in fracture aperture reduced bioclogging in the fracture and then promoted calcite precipitation in fractures.

Figure 8(b) shows the effect of fracture aperture on the Darcy permeability coefficient for fractured rock. Before

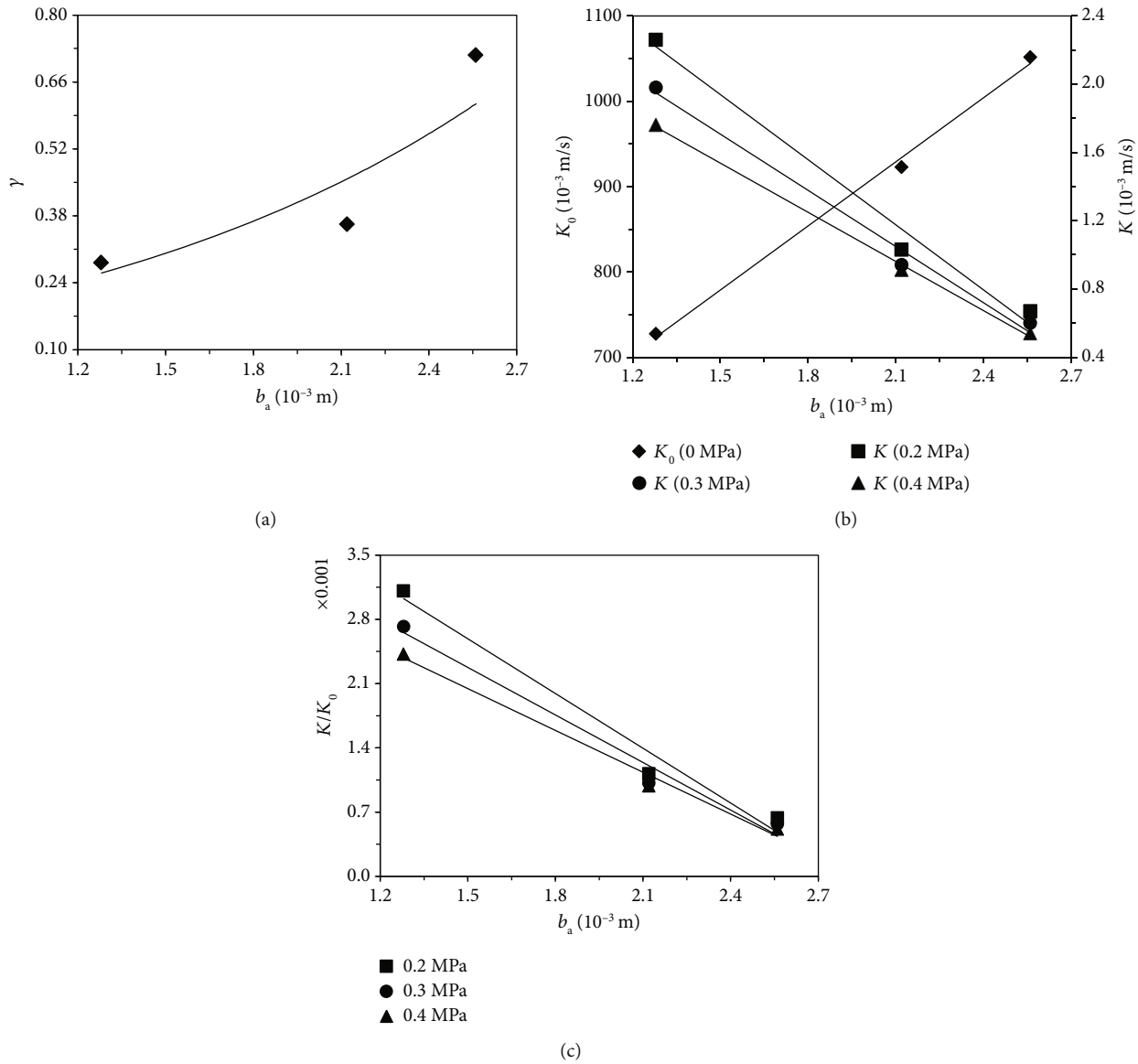

Figure 8: Effect of fractured rock fracture aperture: (a) grouting ratio, (b) permeability, and (c) permeability reduction.

MICP grouting, K_0 increased linearly with the increase in fracture aperture. However, after MICP grouting, K decreased linearly with the increase in fracture aperture. The higher the confining pressure, the smaller the Darcy permeability coefficient.

Figure 8(c) plots the effect of fracture aperture on the permeability reduction of MICP. In Figure 8(c), the permeability reduction increased with an increase in fracture aperture, ranging from 1.28 mm to 2.56 mm. However, more experimental studies will be needed when other fracture apertures and grouting strategies are chosen. Wanniarachchia et al. [17] and Wang et al. [18] studied the seepage characteristics of fractured rock with different fracture apertures numerically. With an increase in fracture aperture, the permeability was gradually reduced. It is essential to consider the hydraulic aperture of fractures in flow calculations, as well as fracture apertures. These conclusions were verified by the analyses in this paper. As fracture apertures (b_a) increased, the permeability coefficient of fractured rock without MICP increased. However, the permeability coefficient decreased in the fractured rock with MICP. The hydraulic aperture is closely related to permeability coefficient.

4.3. Relationships between EIS Response, Grouting Ratio, and Permeability Coefficient of MICP Grouted Fractured Rock. Figure 9(a) plots the relationship between ρ/S and MICP grouting ratio. Obviously, the MICP grouting ratios decreased with an increase in ρ/S. This was because a large grouting ratio resulted in uniform and dense calcium carbonate precipitation in the sample fractures and induced good conductivity. For example, when the grouting ratio was more than zero, the resistivity of calcite in the fracture was about $1 \sim 9 \times 10^3\ \Omega/\mathrm{m}$; however, when the grouting ratio was zero, the resistivity of the fracture was that of the air in the fracture,

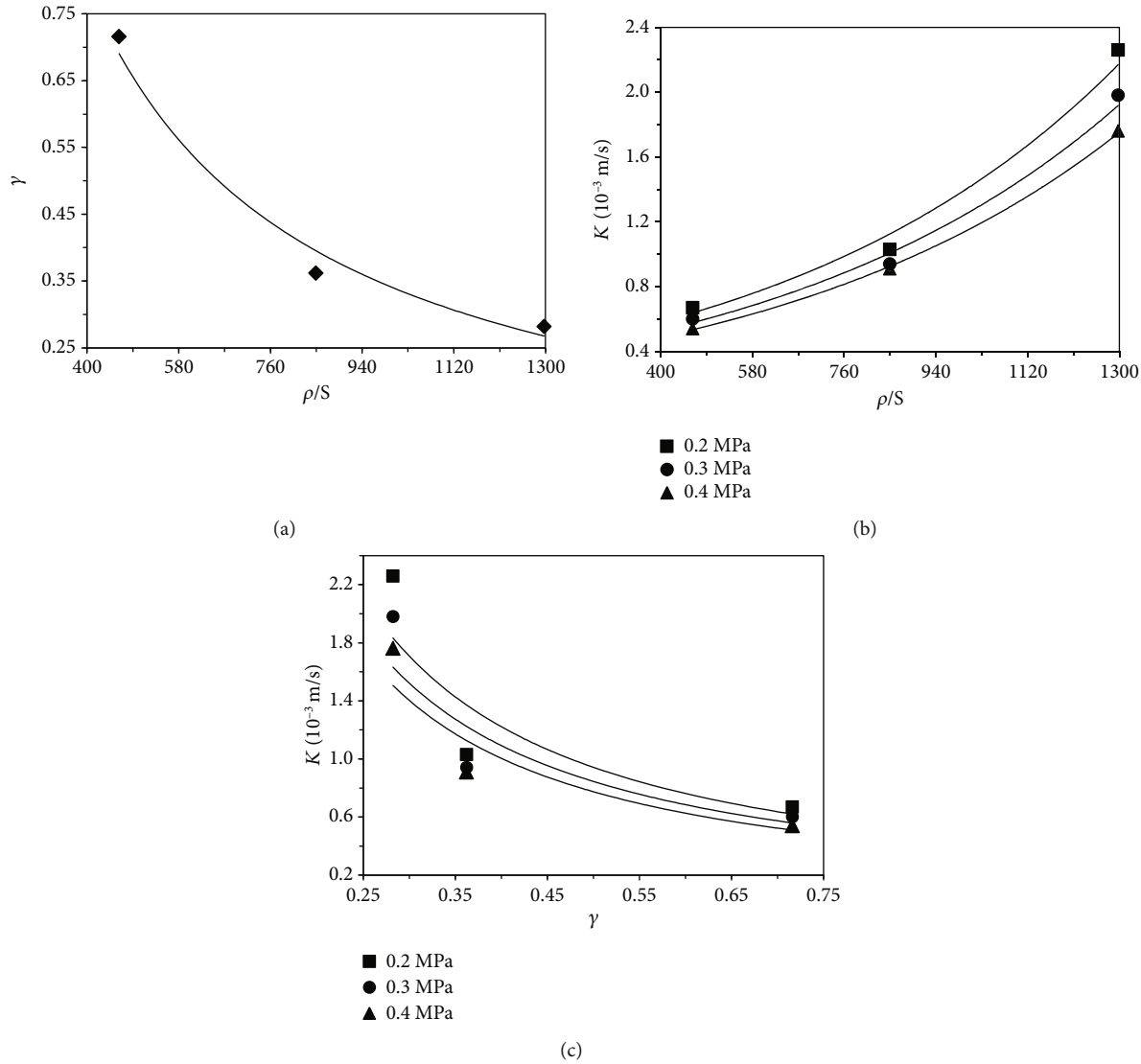

Figure 9: Relationships among K, γ, and ρ/S: (a) γ, (b) K, and (c) K vs. γ.

with a magnitude of $3 \times 10^{13}\ \Omega/\text{m}$. So, it could be deduced that the equivalent circuit model of fractured rock with MICP presented, could depict the characteristics of fractured rock structure. The variance of the calculated parameters of an equivalent circuit model (ρ/S) could well characterise the effect of MICP on fractured rock.

The relationship between ρ/S and the Darcy permeability coefficient of fractured rock with MICP is shown in Figure 9(b). The Darcy permeability coefficient increased with an increase in ρ/S. Based on Figure 9(a), the increase in ρ/S meant a decrease of calcium carbonate precipitation in the fracture and the decrease of precipitation induced an increase in the permeability of the fractured rock sample.

Figure 9(c) shows the relationship between MICP grouting ratio and the Darcy permeability coefficient with MICP. According to Figure 9(c), as the grouting ratio increased, the permeability coefficient decreased. The slope of the permeability coefficient also decreased with increasing grouting ratio. When the grouting ratio reached 60%, the increase of grouting ratio was not obviously decreasing the permeability coefficient. On the other hand, the permeability coefficient decreased with an increase in confining pressure, at constant ρ/S.

4.4. Relationship between Permeability Reduction, EIS, and Grouting Ratio. The relationship between permeability reduction (K/K_0) and the grouting ratio is shown in Figure 10(a). This strongly demonstrates that the permeability reduction of MICP increased with the grouting ratio. This is due to the fact that increasing grouting ratios increased the uniformity and density of calcium carbonate in fractures, reducing the Darcy permeability coefficients of grout-fractured rocks and thus increasing permeability reduction of MICP.

Figure 10(b) shows the relationship between the permeability reduction and ρ/S of fractured rock samples. The

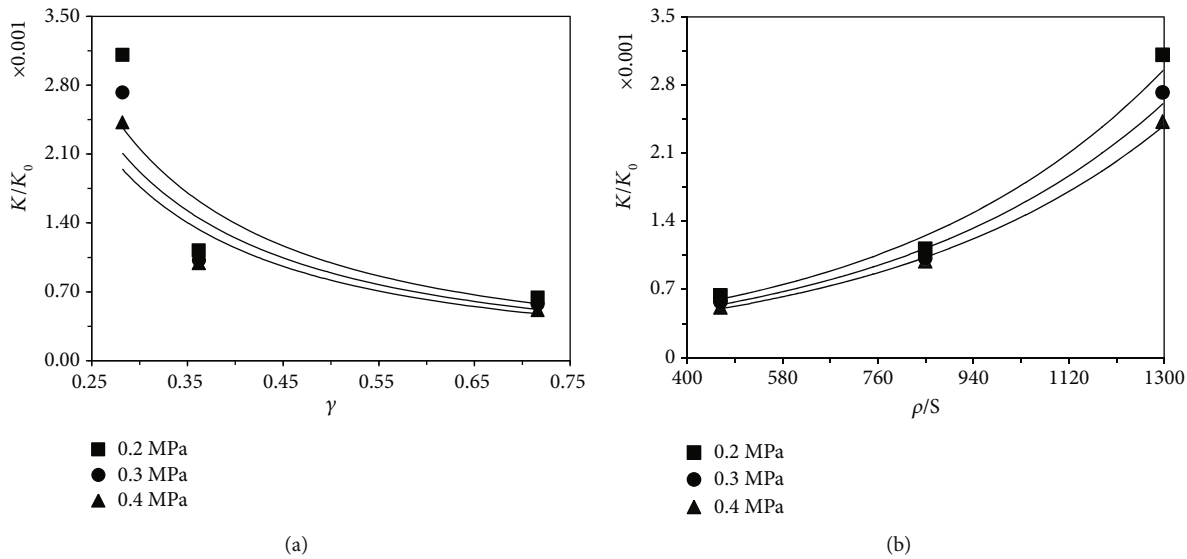

Figure 10: Relationship between permeability reduction and ρ/S and grouting ratio: (a) grouting ratio and (b) ρ/S.

permeability reduction increased with a decrease in ρ/S. According to Figure 9, with a decrease in ρ/S, the Darcy permeability coefficient decreased, which meant an increase in permeability reduction.

In the study by [13], they also showed that the permeability reduction (along both the surface flow and channel flow) was reduced, with an increase of grouting ratio of MICP. Therefore, the accuracy of the above analysis can be reasonably guaranteed. EIS has been used in the measurement of concrete crack width, and electrical conductivity was observed to increase with an increase in crack width [32]. This showed that a relationship can be established between electrical conductivity and the physical characteristics of fractured rock. The relationship between electrochemical properties and permeability established in this paper was a novel application of EIS.

4.5. K and K/K_0 Fitting with Confining Pressure and EIS. For the samples with MICP, the Darcy permeability coefficient K and the permeability reduction (K/K_0) were fitted with ρ/S and confining pressure, and can be presented as follows:

$$K = \frac{-0.95 + 3.2\rho/S - 2.13(\rho/S)^2 + 0.09X_1 - 0.08X_1^2}{1 - 9.28\rho/S + 0.113X_1}, \quad (R = 0.94),$$
$$\frac{K}{K_0} = \frac{7.66\rho/S - 0.0026X_1 + 0.0035X_1^2}{1 + 0.0108\rho/S - 7.559(\rho/S)^2 + 4.186X_1}, \quad (R = 0.99), \tag{7}$$

where X_1 is the confining pressure, with a range from 0.2 MPa to 0.4 MPa, and R is the correlation coefficient.

Therefore, for the fractured rock with MICP, the K and K/K_0 could be predicted by the electrical resistivity, cross-section area of fracture, and confining pressure, with correlation coefficients of 0.94 and 0.99, respectively. Considering that the measurement of electrical resistivity of fractured rock was easier than that of permeability, this paper provides a new method of predicting the permeability reduction in MICP grout-fractured rock by the EIS technique, under conditions of confining pressure.

Only the permeability was considered in the present study. However, mechanical properties of MICP-grouted rock should be analysed in order to evaluate the engineering application value of MICP. The shear strength parameters of fractured rock with MICP will be studied in future research.

5. Conclusions

The permeability reduction and electronic impedance of fractured rock, grouted by MICP, were investigated, considering the effect of confining pressure and fracture aperture. An equivalent circuit model of fractured rock with MICP was presented. The relationships of the Darcy permeability coefficients, permeability reduction, EIS response (ρ/S), and grouting ratios of fractured rocks were discussed. The conclusions are drawn as follows:

(1) The MICP reduced the Darcy permeability coefficient of fractured rock by orders of magnitude of three to four, and increasing confining pressure from 0.2 MPa to 0.4 MPa also reduces permeability.

(2) The presented equivalent circuit model of fractured rock with MICP explained the characteristics of the fractured rock structure and can be used to characterise the effect of MICP on fractured rock.

(3) The permeability reduction in fractured rock, grouted by MICP, decreased with an increase in ρ/S , confining pressure, grouting ratio, and fracture aperture ranging from 1.28 to 2.56 mm under a grouting rate of 0.003 ml/s; the corresponding permeability reduction increased.

(4) The permeability reduction and the Darcy permeability coefficient of fractured rock grouted by MICP were closely related to and well predicted by confining pressure and ρ/S.

Data Availability

The data used to support the findings of this study are available from the corresponding author upon request.

Conflicts of Interest

The authors declare that there is no conflict of interest regarding the publication of this paper.

Acknowledgments

This study was funded by the National Natural Science Foundation of China (grant #51674287, #51508579, #51974043, and #51774058), and Chongqing Basic and Frontier Research Project (grant #cstc2018jcyjA3320).

References

[1] S. C. Li, S. G. Song, L. P. Li et al., "Development and application of the fluid-solid coupling model test system for submarine tunnel," *Chinese Journal of Rock Mechanics and Engineering*, vol. 32, pp. 883–890, 2013.

[2] J. L. Ge, "Development and prospect of chemical grouting techniques," *Chinese Journal of Rock Mechanics and Engineering*, vol. 25, pp. 3384–3392, 2006.

[3] Z. Li, H. Liu, Z. Dun, L. Ren, and J. Fang, "Grouting effect on rock fracture using shear and seepage assessment," *Construction and Building Materials*, vol. 242, p. 118131, 2020.

[4] Y. J. Cheng, "Principles and methods of compacting and splitting grouting to reinforce foundations," *J. Chinese Journal of Geotechnical Engineering*, vol. 16, pp. 22–28, 1994.

[5] J. G. Cheng and J. F. Zhang, "Effects of mechanical response of fillings on fracture flow," *J. Chinese Journal of Rock and Soil Mechanics*, vol. 27, pp. 577–580, 2006.

[6] J. K. Mitchell and C. Santamaria, "Biological considerations in geotechnical engineering," *J. Journal of Geotechnical and Geoenvironmental Engineering*, vol. 131, pp. 1222–1233, 2005.

[7] J. T. DeJong, K. Soga, E. Kavazanjian et al., "Biogeochemical processes and geotechnical applications: progress, opportunities and challenges," *Géotechnique*, vol. 63, pp. 287–301, 2013.

[8] S. Kim, M. Tentzeris, G. Jin, and S. Nikolaou, "Factors affecting efficiency of microbially induced calcite precipitation," *Journal of Geotechnical and Geoenvironmental Engineering*, vol. 138, pp. 992–1001, 2012.

[9] D. Liu, A. Shao, C. Jin, and L. Yang, "Healing technique for rock cracks based on microbiologically induced calcium carbonate mineralization," *Journal of Materials in Civil Engineering*, vol. 30, pp. 82–86, 2018.

[10] M. O. Cuthbert, L. A. Mcmillan, S. Handley-Sidhu, M. S. Riley, D. J. Tobler, and V. R. Phoenix, "A field and modeling study of fractured rock permeability reduction using microbially induced calcite precipitation," *Environmental Science & Technology*, vol. 47, pp. 13637–13643, 2013.

[11] A. J. Phillips, A. B. Cunningham, R. Gerlach et al., "Fracture sealing with microbially-induced calcium carbonate precipitation: a field study," *Environmental Science & Technology*, vol. 50, pp. 4111–4117, 2016.

[12] J. Tobler, M. Dominique, J. M. Minto, G. El Mountassir, R. J. Lunn, and V. R. Phoenix, "Microscale analysis of fractured rock sealed with microbially induced $CaCO_3$ precipitation: influence on hydraulic and mechanical performance," *Water Resources Research*, vol. 54, no. 10, pp. 8295–8308, 2018.

[13] C. Wu, J. Chu, S. Wu, and Y. Hong, "3D characterization of microbially induced carbonate precipitation in rock fracture and the resulted permeability reduction," *Engineering Geology*, vol. 249, pp. 23–30, 2019.

[14] J. Hommel, E. Lauchnor, A. Phillips et al., "A revised model for microbially induced calcite precipitation: Improvements and new insights based on recent experiments," *Water Resources Research*, vol. 51, pp. 3695–3715, 2015.

[15] J. M. Minto, Q. Tan, R. J. Lunn, G. El Mountassir, H. Guo, and X. Cheng, "Microbial mortar'—restoration of degraded marble structures with microbially induced carbonate precipitation," *Construction and Building Materials*, vol. 180, pp. 44–54, 2018.

[16] S. G. Choi, L. Chang, M. Lee, J.-H. Lee, J.-T. Han, and T.-H. Kwon, "Review on geotechnical engineering properties of sands treated by microbially induced calcium carbonate precipitation (MICP) and biopolymers," *Construction and Building Materials*, vol. 246, p. 118415, 2020.

[17] W. A. M. Wanniarachchia, P. G. Ranjitha, M. S. A. Pereraa, T. D. Rathnaweera, C. Zhang, and D. C. Zhang, "An integrated approach to simulate fracture permeability and flow characteristics using regenerated rock fracture from 3-D scanning: a numerical study," *Journal of Natural Gas Science and Engineering*, vol. 53, pp. 249–262, 2018.

[18] P. F. Wang, W. H. Tan, X. W. Ma et al., "Experimental study of seepage characteristics of consecutive and filling fracture with different roughness levels and gap-widths," *J. Rock and Soil Mechanics*, vol. 40, pp. 3062–3070, 2019.

[19] Y. Zhang, *Experimental Study on Microorganism Used for Cementing Sand Soil and Repairing Concrete Cracks*, Tsinghua University, Beijing, 2014.

[20] D. Ma, X. X. Miao, Z. Q. Chen, and X. B. Mao, "Experimental investigation of seepage properties of fractured rocks under different confining pressures," *Rock Mechanics and Rock Engineering*, vol. 46, pp. 1135–1144, 2013.

[21] Y. Ju, Q. G. Zhang, Y. M. Yang, H. P. Xie, F. Gao, and H. J. Wang, "An experimental investigation on the mechanism of fluid flow through single rough fracture of rock," *Science China Technological Sciences*, vol. 56, pp. 2070–2080, 2013.

[22] Y. L. He, Y. J. Tao, and L. Z. Yang, "Experimental study on seepage characteristics of single crack with different joint roughness coefficients," *J. Chinese Journal of Rock Mechanics and Engineering*, vol. 29, pp. 3235–3240, 2010.

[23] T. Miao, B. Yu, Y. Duan, and Q. Fang, "A fractal analysis of permeability for fractured rocks," *International Journal of Heat and Mass Transfer*, vol. 81, pp. 75–80, 2015.

[24] J. M. Minto, E. MacLachlan, G. El Mountassir, and R. J. Lunn, "Rock fracture grouting with microbially induced carbonate precipitation," *Water Resources Research*, vol. 52, no. 11, pp. 8827–8844, 2016.

[25] S.-G. Choi, K. Wang, Z. Wen, and J. Chu, "Mortar crack repair using microbial induced calcite precipitation method," *Cement and Concrete Composites*, vol. 83, pp. 209–221, 2017.

[26] G. Nover, S. Heikamp, and D. Freund, "Electrical impedance spectroscopy used as a tool for the detection of fractures in

rock samples exposed to either hydrostatic or triaxial pressure conditions," in *Natural Hazards*, G. A. Papadopoulos, T. Murty, S. Venkatesh, and R. Blong, Eds., vol. 21, pp. 317–330, Springer, Dordrecht, 2000.

[27] P. J. Han, Y. F. Zhang, F. Y. Chen, and X.-h. Bai, "Interpretation of electrochemical impedance spectroscopy (EIS) circuit model for soils," *Journal of Central South University*, vol. 22, pp. 4318–4328, 2015.

[28] H. F. Wang and J. C. Hu, "Research on topological structure of rock electrochemical impedance spectroscopy," *Advanced Materials Research*, vol. 243, pp. 2920–2924, 2011.

[29] H. F. Su, Z. L. Ren, A. S. Menmo et al., "Investigating drying behavior of cement mortar through electrochemical impedance spectroscopy analysis," *Construction and Building Materials*, vol. 135, pp. 361–368, 2017.

[30] W. Q. Zhang, H. T. Zhou, and W. H. Guo, "Experimental study on seepage characteristics of fractured rock mass and its electrical response," *Journal of Hydrologic Engineering*, vol. 24, no. 7, article 04019017, 2019.

[31] M. Zhang, "Theory and apparatus for testing low-permeability of rocks in laboratory," *Chinese Journal of Rock Mechanics and Engineering*, vol. 22, pp. 919–925, 2013.

[32] A. Akhavan and F. Rajabipour, "Quantifying permeability, electrical conductivity, and diffusion coefficient of rough parallel plates simulating cracks in concrete," *Journal of Materials in Civil Engineering*, vol. 29, no. 9, article 04017119, 2017.